Astronomy & Astrophysics manuscript no. paper7˙bs2 June 10, 2005
(DOI: will be inserted by hand later)

A multiline study of flows of the M 1.0 flare on October 22, 2002

G. Del Zanna[1⋆], A. Berlicki[2,3], H. E. Mason[4], and B. Schmieder[2,5]

[1] MSSL, University College London Holmbury St. Mary Dorking UK RH5 6NT
[2] Observatoire de Paris, Section de Meudon, LESIA, F-92195 Meudon Principal Cedex, France
[3] Astronomical Institute of the Wrocław University, ul. Kopernika 11, 51-622 Wrocław, Poland
[4] Department of Applied Mathematics and Theoretical Physics, University of Cambridge, Cambridge UK CB3 0WA
[5] Institute of Theoretical Astrophysics, University of Oslo, Blindern, N-0315 Oslo, Norway

June 10, 2005

Abstract. In this paper we present a further study of the M1 class flare observed on October 22, 2002. We focus on the SOHO Coronal Diagnostic Spectrometer (CDS) spectral observations and the ground-based (VTT/MSDP) observations performed during a multi-wavelength campaign with TRACE. Strong blue-shifts are observed in the CDS coronal lines in flare kernels during the impulsive phase of this flare. From a careful wavelength calibration we deduce upflows of 140 km/s for the Fe XIX emission, less for the cooler lines and downflows in the He I line (13 km/s). The upflows correspond to full shifts of the line profiles. The large line-widths, specially for the Fe XIX line indicate the existence of strong turbulence velocities. These flows are observed at the launch time of the flare, and correspond to the "explosive evaporation". The location of these blueshifted kernels, few arc seconds far from the flare onset location is explained by the chain reaction of successive magnetic reconnections of growing emerging field line with higher and higher overlaying field. This interpretation is evidenced by the analysis of the magnetic topology of the active region using a linear force-free-field extrapolation of THEMIS magnetogram. In other kernels reached during the late phase of the flare by CDS we observed small upflows (maximum 50 km/s) which we interpreted as due to "gentle evaporation".

Key words. Sun: corona – Techniques: spectroscopic – Line: profiles

1. Introduction

The broadening and blue-shifting of spectral lines for high temperature emission during the initial phase of solar flares has been extensively studied in the X-ray wavelength range using data from SOLFLEX (cf. Doschek et al. 1979), the Solar Maximum Mission's (SMM's) X-ray polychromator (XRP) Bent Crystal Spectrometer (BCS) (cf Antonucci et al. 1982) and the BCS on YOHKOH (see, e.g., Bentley et al. 1994). Plasma velocities deduced from Doppler-shift analysis were of the order of a few hundreds km s^{-1}. This blueshifted emission was interpreted as evidence for chromospheric evaporation. However, these BCSs had no spatial resolution, so it was not possible to locate the source of the blueshifted X-ray emission, or to spatially separate this from any stationary components. A further complexity in the interpretation of BCS spectra was due to the superposition (at different wavelengths) of stationary components originating from different locations. In general asymetric line profiles were observed, rather than totally shifted lines. Without spatial resolution in the BCS X-ray observations, any weak blueshifted X-ray emission would swiftly be swamped by the strong stationary emission from the flare X-ray loops. In a recent paper, Warren & Doschek (2005) interpret these blue-shifted asymetries as a succession of independently heated threads within flare loop structures. To progress further, it is essential to spatially locate the high temperature blue shifted emission in relation to the flare loops and structures.

The SMM XRP Flat Crystal Spectrometer (FCS) had a limited spatial resolution (14″). Zarro et al. (1988) reported spatially confined Mg XI blue-shifted emission during the impulsive phase of a small flare. The Fe XXI line at 1354.1 Å emitted at about 10^7 K, was studied with the SMM Ultraviolet Spectrometer and Polarimeter (UVSP) instrument (with spatial resolution down to 3″) . Mason et al. (1986) deduced upward flows in Fe XXI emitting plasma in excess of 200 km/s. Their observations supported the hypothesis of chromospheric evaporation in the

Send offprint requests to: G. Del Zanna
(G.Del-Zanna@damtp.cam.ac.uk)
⋆ Previous address: DAMTP, University of Cambridge

'footpoint region' of what subsequently became soft X-ray emitting loops.

The Coronal Diagnostic Spectrometer (CDS) instrument on SOHO has the capability to simultaneously obtain spatial and spectral information for emission over a wide range of plasma temperatures. One of the hottest lines recorded with CDS is the Fe XIX flare line at 592.2 Å. This is formed at a temperature around 8×10^6 K. Using CDS, it is possible to locate the source of high temperature blue-shifted emission seen during a solar flare. Czaykowska et al. (1999) reported SOHO/CDS observations of blue-shifts in Fe XVI (3×10^6 K) and Fe XIX (8×10^6 K) lines. These observations were however performed more than one hour after the maximum of a two-ribbon M6.8 flare. The blue-shifts appeared to be located at the outer edges of the flare ribbons.

Spatially-resolved spectral information from CDS were reported by Del Zanna et al. (2002a) covering the entire evolution of a small flare. Long-lasting (over an hour) blue-shifts of 30 km/s in coronal lines (Mg X, Si XII, emitted at 1-2 MK) were located at the footpoints of a small loop system. These could be interpreted as indirect evidence of chromospheric evaporation.

Recently, Teriaca et al. (2003) published CDS and ground-based observations of an eruptive C2 flare. The main findings were quasi-simultaneous and co-spatial measurements of upflows in the flare line (Fe XIX) and downflows in the chromosphere, as seen in the He I 10830 Å line. Brosius & Phillips (2004) presented CDS observations of a larger M6 flare. These authors kept the position of the CDS slit fixed, thus sacrifying spatial coverage in favour of a high (10s) time resolution. They used TRACE observations to track the evolution of the flare. Their main results were measurements of upflows ($\simeq$60 km/s) in flare lines and downflows ($\simeq$40 km/s) in cooler transition region lines during the impulsive phase. The X-ray emission appeared $\simeq$1m after the start of the impulsive intensity rise in the cooler lines. They concluded that their observations were consistent with non-thermal particles transferring most of the energy into the chromosphere and creating these oppositely-directed flows.

The "explosive" evaporation seen in the emission from high temperature flare plasma is thought to be driven by non-thermal electrons accelerated during the primary energy release (Antonucci et al. 1984) and may occur when the heating rate due to collisions of non-thermal electrons with the ambient plasma in upper layers of the chromosphere exceeds the chromospheric radiative losses (Fisher 1987). This occurs when the temperature of the heated region is above 2×10^5 K and thus this kind of evaporation cannot be seen in chromospheric spectral lines which are formed in a cooler plasma.

If a region of the chromosphere heated by non-thermal electrons is thick enough, then the rapid temperature increase produces an enhanced pressure in the heated region. This overpressure, besides the evaporation, also drives downward-moving cool and dense *chromospheric condensations* (Fisher et al. 1985a) which seem to be responsible for red-shifts of the Hα line profiles reported by many authors (Svestka 1976, Ichimoto & Kurokawa 1984). Fisher et al. (1985c) modelled the hydrodynamic and radiative response of the atmosphere to short impulsive injections of non-thermal electron beams. They showed that only the high-energy flux of non-thermal electrons drives explosive evaporation, accompanied by the formation of cool chromospheric condensations in the flare chromosphere.

A coordinated observational campaign was organised to follow the evolution of the NOAA 0162 active region during October 22, 2002. Ground based instruments (THEMIS and Vacuum Tower Telescope - VTT - on Tenerife, Canary islands, Spain) and space observatories (SOHO, TRACE and RHESSI) were involved. The active region had several flares, including an M1 flare. The morphology and evolution of the M1 flare in particular during the gradual phase (when RHESSI was observing) were presented in Berlicki et al. (2004). Here, we focus in particular on the nature of the emission from the high temperature plasma, as seen in the initial phase of the M1 flare with the CDS on SOHO.

In this paper we focus primarily on the nature of the blue shifted emission from high temperature plasma and its relationship with the cool chromospheric emission and the hot flare emission. In Sect. 2 we summarise the observing campaign for the 22nd October 2002. In Sect. 3 we present the CDS observations and results in detail, paying particular attention to the measurement of wavelength shifts. In Sect. 4 we discuss the magnetic topology of the flare according to a non linear force free field extrapolation of the magnetic field with an observed THEMIS magnetogram as boundary conditions. The flows of the flare plasma are presented and discussed in this context (Sect. 5).

2. Co-ordinated observing campaign for 22nd October 2002

The active region NOAA 0162 was mainly bipolar, quite extended, and relatively active. It was observed on October 22, 2002 with SOHO, TRACE, RHESSI, and from the ground with THEMIS and VTT. The SOHO/CDS sequence of observations was extensive and ran during 08:02-13:07 UT and 15:18-18:13 UT (see Table 1). The CDS observations, described in detail below, consisted of 'rasters' during which the slit was scanning the active region.

During October 22 the active region produced at least 3 flares. The main M1 flare occurs at 15:30 UT during the CDS raster at 15:18:16–15:43:16 UT. Fig. 1 shows the X-ray light curves from GOES 8 during the CDS scan. The time derivative of the 0.5–3 Å light curve can be used as a proxy for the hard X-ray emission, and indicates a peak at 15:33 UT. The timings of some CDS slit positions and some TRACE and ground-based observations are also shown.

VTT/MSDP observations in Hα consisted of 9 raster scans between 15:30 and 16:17 UT and a field-of-view of

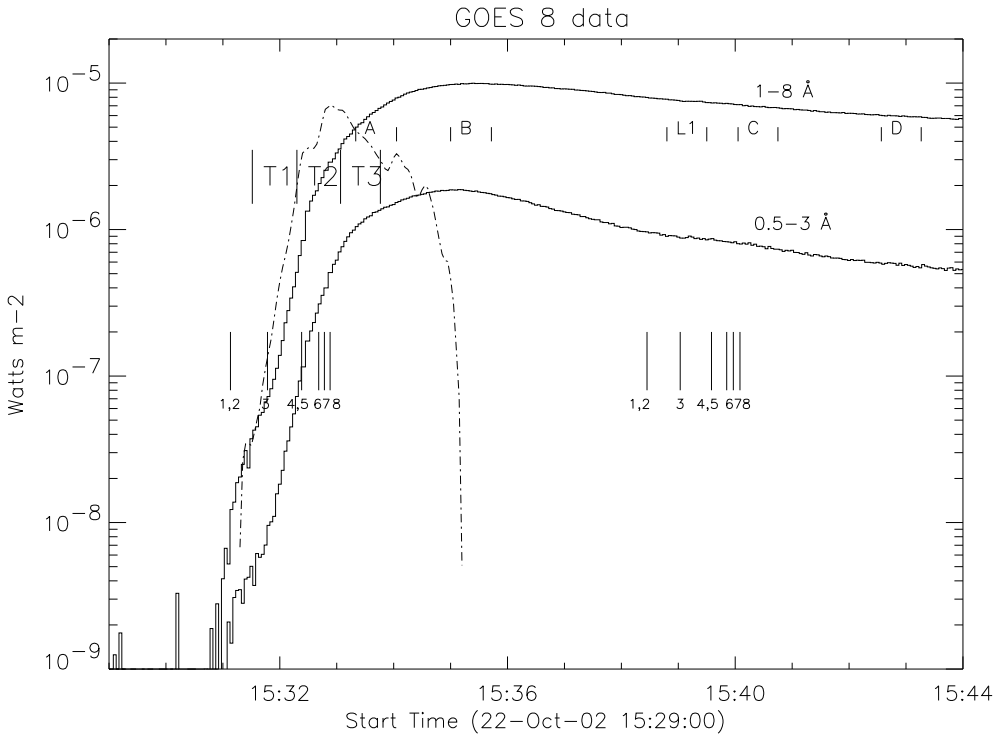

Fig. 1. Time evolution of the GOES 8 X-ray fluxes on October 22, 2002 during the M1 flare and the CDS raster scan. The dot-dashed curve is the time derivative of the 0.5–3 Å light curve, and can be used as a proxy for the hard X-ray emission. The timings of a few key observations are indicated (top: CDS slit positions, see Fig. 3; middle: TRACE images, see Fig. **??**; bottom: Hα slit positions during two consecutive rasters, see Fig. 10).

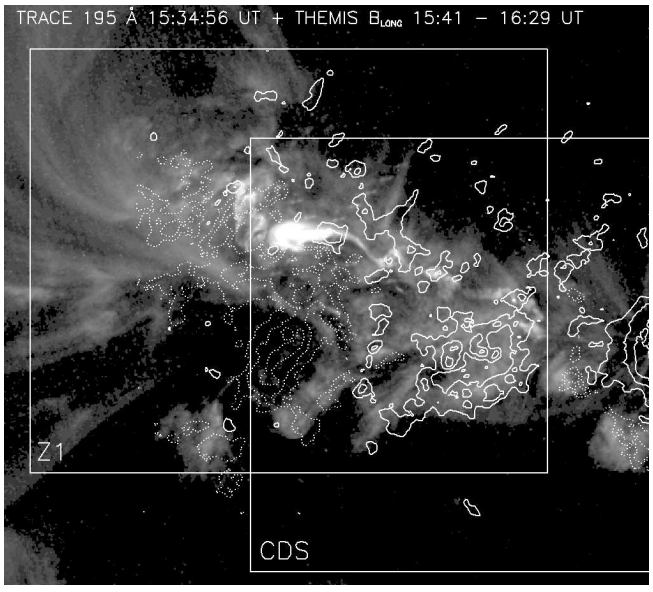

Fig. 2. TRACE 195 Å image of the active region during the M1 flare. with contours (± 200, 500, 1000 G) from the THEMIS magnetogram obtained in the Na D1 line. The fields of view of the TRACE sequence of images (Z1, see Fig. 3), of the region of the M1 flare and of the CDS raster are also shown.

about 380"×170" (exposure time of 0.5s). The rastering was performed from east to west, in the opposite direction compared to CDS. Below we will concentrate on the first VTT spectral raster, which scanned the active region during 15:30-15:37 UT, i.e. in the impulsive phase. Results from the follow-up raster (gradual phase) have been presented by Berlicky et al. (2005).

Table 1. CDS rasters analysed - 22 Oct 2002.

Time (UT)	CDS files	CDS study
8:02:50–8:27:54	s26053r00	SIG_FT44
	s26054r00	ARDIAG_2
	s26054r01	ARDIAG_2
	s26055r00	ARDIAG_2
	s26056r00	SIG_FT44
15:18:16–15:43:16	s26058r00	SIG_FT44
15:43:30–17:07:33	s26059r00	ARDIAG_2
17:08:03–18:32:46	s26059r01	ARDIAG_2

TRACE 195 Å images were obtained at high-cadence (40 s) between 15:29 and 15:41 UT (with a FOV 384"×384" and a 1" resolution)(see Fig. 2 for the full TRACE FOV). Before and after this time the TRACE observations were obtained with slightly lower time resolution (50 s) and larger FOV (512"×512").

Fig. 3 shows a sequence of TRACE 195 Å difference images in the central part of the TRACE FOV, where the flare took place. The location and timings of the CDS slit are also indicated in Fig. 3. The first obvious signature

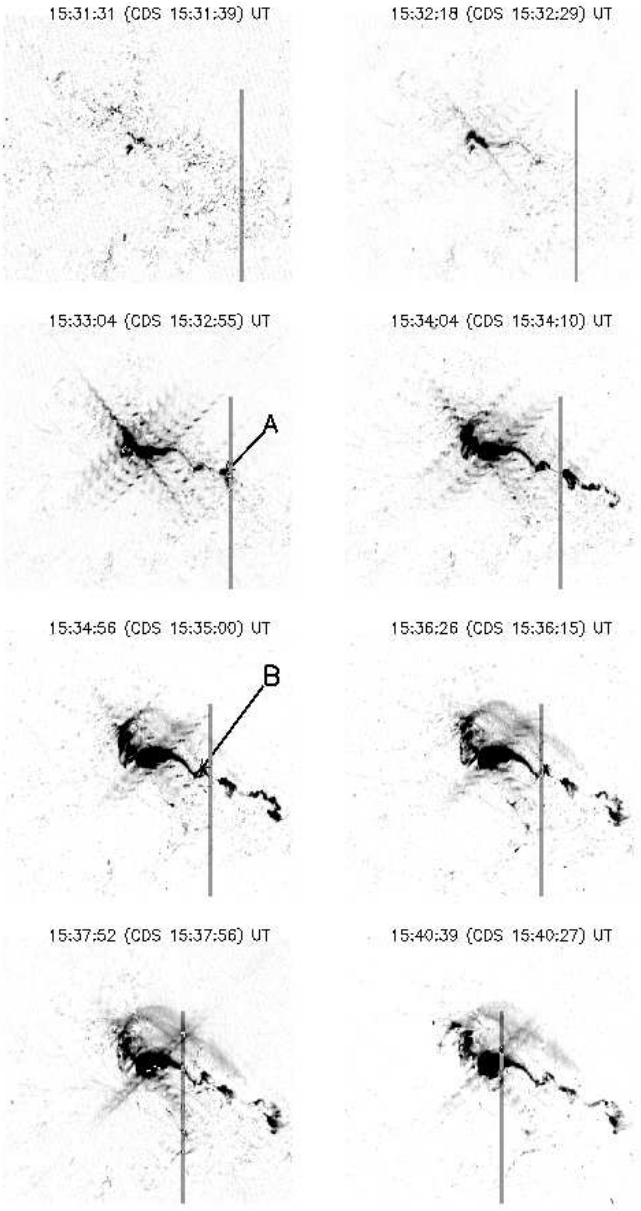

Fig. 3. Sequence of TRACE 195 Å difference images (negative) of the region Z1 (cf. Fig. 2) and centred during the peak of the M1 flare. The image that has been subtracted was taken at 15:29:59 UT, before the start of the flare. The timings indicate the initial exposure time for each TRACE image, and the corresponding nearest CDS exposure. The location of the CDS slit is also shown.

in the TRACE 195 Å occurs at 15:32:18 UT, somewhat later than the increase in the GOES X-ray flux. However, a small brightening already appears at the same location on the 15:31:31 UT TRACE image.

By 15:33 UT, the entire ribbon structures (located on either side of the neutral line) brighten up in the TRACE 195 Å image. The Hα ribbons were already visible at 15:31 UT (see Berlicki et al. 2004).

CDS had the slit positioned over the main area of the flare during the peak and gradual phase (cf. Fig. 1 and Fig. 3) and can therefore be used to estimate the temperatures of the various features recorded by TRACE. As shown below, CDS observed strong Fe XIX emission in the locations of both the ribbons and the higher-lying loops observed by TRACE, which suggests that most likely the TRACE images are dominated by hot emission from Fe XXIV.

.

Table 3. Some of the prominent lines in the CDS/NIS wavelength bands, used in this paper. Wavelengths are taken from the CHIANTI database unless otherwise stated. Those indicated with an asterisk have been used for the wavelength calibration. When only one decimal place is indicated, the lines are blends of at least two transitions. The approximate temperature of maximum ion abundance (in ionization equilibrium) is also indicated, together with the channel and the CDS study that recorded the lines (FR: fast raster; DR: diagnostic raster, see text).

Ion	wavelength (Å)	log T_e	NIS	
Si X	347.402	6.1	1	FR,DR
Si X	356.0	6.1	1	FR,DR
Si XII	520.665*	6.3	2	FR,DR
He I	522.210*	4.5	2	FR,DR
O IV	553.34*	5.3	2	FR,DR
O IV	554.076	5.3	2	FR,DR
O IV	554.513	5.3	2	FR,DR
O IV	555.263*	5.3	2	FR,DR
Fe XIX	592.16	6.9	2	FR,DR
Fe XII	592.60*	6.1	2	FR,DR
Mg X	624.941*	6.0	2	FR,DR
O IV	625.853	5.3	2	FR,DR
O V	629.732*	5.4	2	FR,DR

3. CDS instrument and data analysis

The CDS observations were performed with the normal incidence spectrometer (NIS). The internal scan mirror allows CDS to scan an area of 4′ square within a single 'raster', from west to east. The N-S coverage was provided by the use of the long slit 4″x240″.

The NIS is composed of two gratings, that produce two wave-bands (NIS 1: 308 – 379 Å and NIS 2: 513 – 633 Å;).

The CDS observing sequences were specifically designed to study the spatial and spectral characteristics of small flares. They included a range of spectral lines from different ions and in particular the high temperature flare line, Fe XIX 592.2 Å. CDS observed NOAA 0162 with the two types of rasters (see Table 1): 1) a slow diagnostic raster (1hour 20 m, CDS study name ARDIAG_2) that extracts many diagnostic lines; 2) a fast raster (slit exposure of 18s for a total duration of 20 m, CDS study name SIG_FT44) that only extracts a few lines, selected to cover a wide range of temperatures (see Table 3).

One important aspect of CDS is that lines emitted from the chromosphere up to the corona are observed. This is very useful for a proper co-alignment with other datasets, e.g. photospheric magnetic fields from

Table 2. List of the main lines used for the wavelength calibration. The first row gives the reference wavelengths (λ_{st}, Å) adopted. The second row gives the wavelengths (λ_1, Å) as obtained from the pre-flare raster s26055 and the calibration curve adopted. The third row gives the corresponding relative velocities (v_1, km/s). The following two rows give wavelengths (λ_2, Å) and relative velocities (v_2, km/s) as obtained from the post-flare raster s26059 and using the same calibration curve. Note the small differences in the measured wavelengths, giving confidence in the stability of the wavelength calibration.

	Si XII	He I	Ne IV	Al XI	O IV	O IV	Ca X	Ne VI	Ne VI	Fe XII	Mg X	O V
λ_{st}	520.665	522.210	542.07	550.06	553.34	555.263	557.765	558.594	562.803	592.60	624.941	629.732
λ_1	520.675	522.208	542.031	550.070	553.365	555.252	557.758	558.590	562.791	592.590	624.936	629.735
v_1	5	-1	-21	5	13	-6	-3	-2	-6	-5	-2	1
λ_2	520.664	522.211	542.061	550.066	553.354	555.260	557.769	558.622	562.812	592.597	624.932	629.747
v_2	0	0	-4	3	7	-1	1	15	5	-1	-4	6

SOHO/MDI, and coronal images from TRACE. A series of standard corrections was applied to the raw NIS data. These include de-biasing, flat-fielding, corrections for the burn-in of the lines and high count rates, cosmic ray removal. Multiple-line-fitting techniques have been used to determine the moments of each of the spectral lines in the spectra by removing the *'continuum'* intensity, which is mainly due to scattered light in the NIS. In SOHO post-recovery spectra, the CDS/NIS line profiles are no longer gaussians, and show a broadened and asymmetrical long wavelength wing, which is approximately constant and can therefore be accounted for. The CDS calibration of Del Zanna et al. (2001) has been adopted here, with a correction to take into account the effects on the NIS detector of the gain depression caused by exposures with the wide slit.

3.1. Wavelength calibration

For a correct interpretation of the velocities observed, an accurate wavelength calibration is necessary. CDS does not have an absolute wavelength calibration. Changes in the wavelength calibration have been observed (up to 0.1 Å in NIS 2), and caused primarily by on-board temperature changes (and their history), which are due to the variable illumination received from the Sun (D. Pike, priv. comm.). Also, the wavelength calibration often requires a 'scan mirror correction', which also appears to vary. In addition, there are no photospheric or chromospheric lines within the CDS wavelength bands (except He I).

The above means that the calibration has to be done using the observed transition region and coronal lines, and that it is necessary to obtain/check the wavelength calibration for each set of observations.

For the calibration, it is important to have accurate 'standard' rest wavelengths for the spectral lines concerned, which is a non-trivial issue if very accurate measurements are sought. We have adopted the values shown in Table 3. For most lines we adopt the wavelengths as in the CHIANTI database, which in turn has values mostly from NIST. We note, however, that the values in NIST are taken from the literature, where many measurements have been obtained from solar spectra and present some inconsistency.

The case of the important Fe XIX 592.2Å line is emblematic. Our calibration, based on a small sample, provides a wavelength of 592.16 Å, in excellent agreement with the accurate measurements of Widing (1978), but different from e.g. the value previously reported by Sandlin et al. (1976), 592.24 Å. We note that Widing (1978) averaged many flare observations taken with the NRL spectroheliogram on Skylab. On the other hand, Lawson & Peacock (1980), in their review of the $n = 2 \rightarrow n = 2$ transitions, based on solar and laboratory measurements, suggested an energy for the $2s^2\ 2p^4\ {}^1\mathrm{D}_2$ level of 168770 cm^{-1}. This energy is equivalent to a rest wavelength of 592.522 Å, i.e. at the considerable difference of 183 km/s, compared to our result, 592.16 Å. An extra complication is due to the presence, in the red wing of the Fe XIX line, of a coronal line only recently identified as due to Fe XII (see Fig. 8 below and Del Zanna et al. 2002a, Del Zanna & Mason 2004).

To calibrate the CDS observations, average CDS spectra containing a large number of lines (the diagnostic rasters) of two rasters taken before and after the flare have been analysed and wavelength-calibrated. We assumed for the CDS pixel-wavelength calibration a quadratic function. The wavelength calibration was remarkably stable over the period. Table 2 shows that in most cases the line centres were within a few km/s the assumed reference values.

In terms of uncertainties, we note that the positions of the line centres can be calculated with approximately 1/10 of a pixel accuracy (1 pixel in the NIS 2 channel is approximately equivalent to 0.11 Å), and the average differences between the predicted and standard wavelengths are of the same order, 0.01 Å. This accuracy results in an uncertainty in the derivation of velocities of the order of 10 km/s. An additional systematic uncertainty is due to the spatially-dependent effects due to the geometrical distortions within the instrument. This is more difficult to quantify, because it depends on the type of relative measurement that is done, but is again of the same order. Finally, we note that the resolution of the CDS instrument

does not allow simultaneous measurements of stationary and non-stationary components. Hence, our results refer in most cases to the average main displacement of each line profile. This is not true in the case of the Fe XIX emission, since it is present only during flares. Significant line broadening can however be measured even in post-recovery spectra.

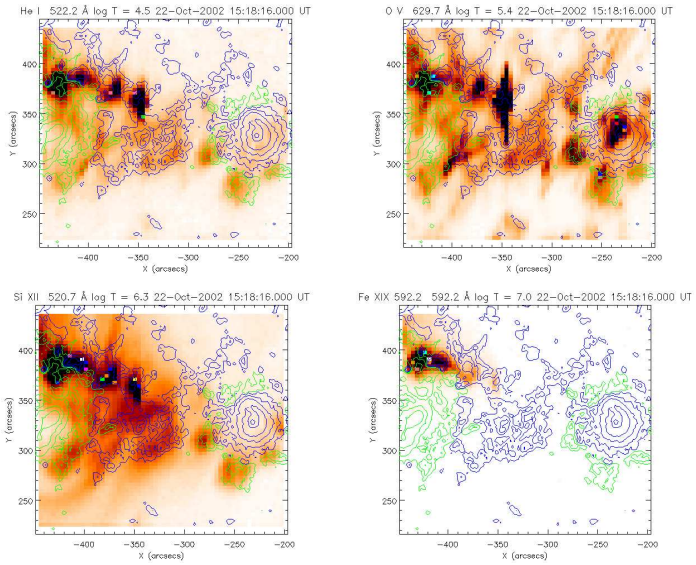

Fig. 4. Monochromatic images obtained from the CDS raster. Contours from the SOHO/MDI magnetograms are superimposed.

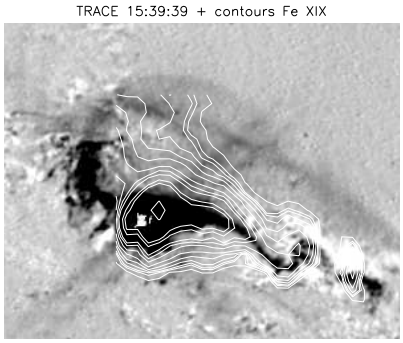

Fig. 5. TRACE 195 Å difference (negative) image with contours of Fe XIX intensity.

3.2. Overview of the CDS results

Fig. 4 shows monochromatic images obtained from the CDS raster, in lines emitted over a broad temperature range. The ribbon structure is so bright in He I and also at transition region temperatures (e.g. O V) that the bright-

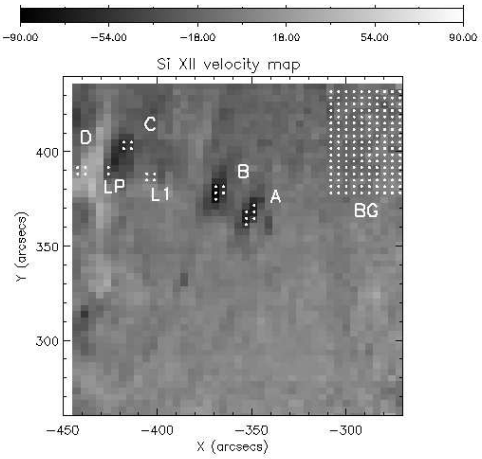

Fig. 6. Si XII λ520.665 Å velocity map in the flare region, with the areas selected for further analysis. Areas A,B,C correspond to regions of strong blue-shifts, while area D of red-shift. Region LP corresponds to the area of peak Fe XIX λ592.16 Å intensity, while region L1 is where the central part of the flare loop is located. Region BG is a 'background' reference region.

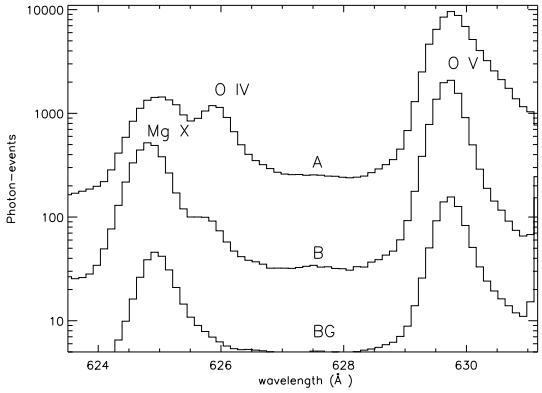

Fig. 7. Spectra of three different regions, A,B,BG. Note that in region A the profiles of the strongest lines are nearly saturated. The O IV line has been used for density measurements at transition-region temperatures.

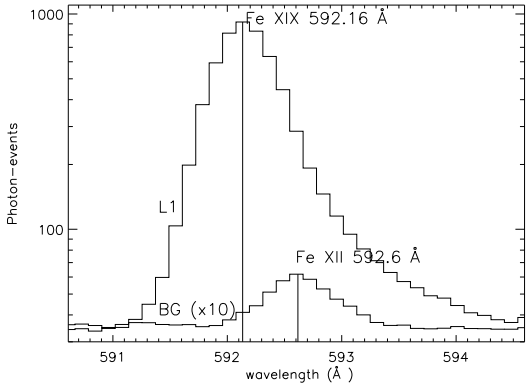

Fig. 8. Spectra of the region L1 (peak flare), and of the background BG (multiplied by ten), showing the Fe XIX λ592.16 Å and the previously unidentified Fe XII line. Outside of the flaring region, all the intensity is due to Fe XII.

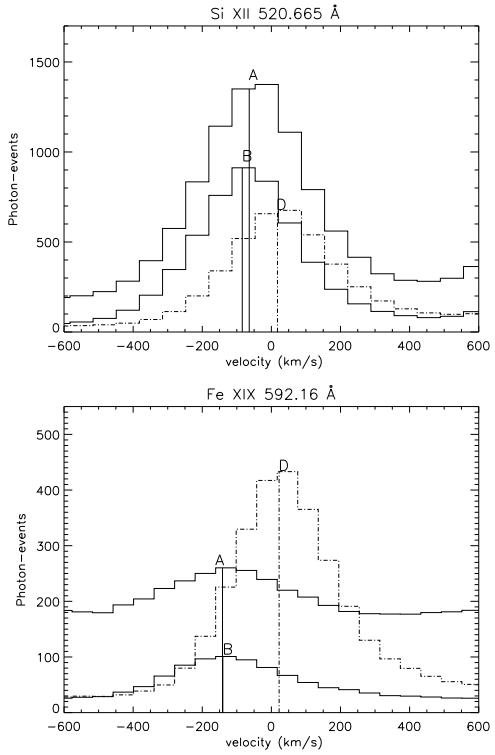

Fig. 9. Line profiles in regions A,B,D showing the evident blue-shifts in the coronal (Si XII) and flare (Fe XIX) lines in regions A,B.

est lines saturated the detector in some positions (region A, defined below). The hot emission from Fe XIX is only present in the ribbon and high-lying loop structures seen in the TRACE 195 Å band (see Fig. 5).

The velocity maps show a consistent pattern. Large velocities, mainly upflows, are only visible in lines formed above 1 MK, and in the Fe XIX flare line. Fig. 6 (top) shows as an example a velocity map in the flare area obtained from a Si XII line, and the regions selected for further study. Line fitting was performed on the averaged spectra of these selected regions. Figs. 7,8,9 show some line profiles in a few selected regions. Table 4 presents some results of the line fitting, in particular velocities, intensities and line widths.

Regions A,B were associated with the brightest emission in the chromospheric-TR lines, and with strong upflows in the Fe XIX flare line. Region A was observed by CDS during 15:33:20–15:34:10 UT (see Fig. 3 for the correspondence with TRACE), i.e. in the impulsive phase of the flare (Fig. 1). Region B was observed during 15:35:00–15:35:50 UT, i.e. at the time of the peak X-ray emission (Fig. 1).

As observed in other cases (Del Zanna et al. 2002b), upflows are also seen in the lower-temperature Si XII and Mg X lines. Our findings are contrary to those of Brosius & Phillips (2004), that discouraged the use of Mg X lines because of blends with O IV emission.

In terms of line widths, aside from a few notable exceptions, the full-width at half maximum ($FWHM$) values are close to the value of the instrumental width (0.5 Å in post-recovery spectra). The exceptions are in regions A,B,D and mostly in the coronal lines. Interestingly, the Fe XIX line has a large width in all of the regions, suggestive of large turbulent motions. As also noted by Brosius & Phillips (2004), the observed blue-shifts are not superimposed on a stationary component, but appear as shifts of the entire line profiles in Mg X, Si XII and Fe XIX (see Fig.9).

We also find upflows (although smaller) in the TR lines in region B. Interestingly, in region A, during the impulsive phase, He I, O IV and O V lines show small downflows. However, these results should be considered with some caution because the detectors were nearly saturated (completely saturated in the O V case).

The other regions were close to the flare site. Region L1 shows near-zero line-of-sight velocities in all lines. The region LP corresponds to the area of peak X-ray emission, as judged from the TRACE 195 Å images and the Fe XIX emission, observed by CDS 7 minutes later, around 15:42 UT. It is interesting to notice that, on the opposite sides of the peak emission, flows of opposite directions are observed (region C, upflow; region D, downflow) in all the lines, emitted from TR to flare temperatures.

Region BG was chosen as a background reference region, not interested by the flare. The lines show near-zero line-of-sight velocities. Note that the intensity of the Fe XIX line is an upper limit (the emission being dominated by the Fe XII). We have compared the line intensities of the background region with other observations of the quiet Sun, and found that, for the transition region lines, the values are very close to those of the average quiet Sun.

The O IV lines (cf. Fig. 7) are an useful density diagnostic at transition region temperatures, and in the locations of strong brightenings. For both the upflow regions A and B we obtain averaged line-of sight electron densities of $\simeq 10^{11}$ cm^{-3}. Interestingly, the two O IV intensities increase respectively by factors of $\simeq$300, 20, while the density increases by an order of magnitude compared to quiet Sun values (cf. Del Zanna & Bromage 1999). This means that the filling factor of the two regions could be different. This is an added complexity that a detailed flare interpretation should take into account.

4. Magnetic topology and Hα ribbons

In Berlicki et al. 2004 we present the magnetic topology of the active region. The magnetic field shows that this active region was highly sheared. The trigger of the flare was the emergence of a locally very twisted magnetic flux (bipole). The linear force-free-field extrapolation of the magnetic field lines obtained from THEMIS magnetogram provides an explanation of the fast propagation of the brightening along the ribbon (of the order of few min) from the emerging dipole towards the leading spot. This propagation can be explained by the reconnection of the growing emerging field lines with the higher and higher overlying

Table 4. Results from the averaged spectra of the various regions displayed in Fig. 6. For each of the selected spectral lines, we display the averaged velocities v (in km/s; negative corresponds to blue-shift), the calibrated line intensities I (erg cm^{-2} s^{-1} sr^{-1}), and the full-width at half maximum $FWHM$ (Å). O IV(a) indicates the 553.4 Å line, while O IV(b) indicates the 625.8 Å line, used to obtain the electron densities N_e (cm^{-3}). Large blue-shifts are mostly observed in regions A,B,C. Note, however, that some of the lines are close to saturation in region A, and values are uncertain (they are indicated in parentheses).

Region	A	B	C	D	L1	LP	BG
He I v	13	-27	-30	-17	-17	-36	-22
I	2393	770	112	377	751	1293	16
$FWHM$	0.61	0.53	0.51	0.56	0.51	0.51	0.50
O IV(a) v	(33)	-21	-24	13	0	-20	0
I	(9818)	598	80	237	252	686	33
O IV(b) I	2333	111	-	-	-	-	-
N_e (O IV)	2 10^{11}	0.9 10^{11}	-	-	-	-	-
O V v	(23)	-25	-21	0	-12	-28	-4
I	(33226)	5038	721	2490	2840	6782	387
$FWHM$	(0.70)	0.50	0.50	0.55	0.50	0.50	0.50
Mg X v	(14)	-62	-51	29	-17	-37	-5
I	(5910)	1630	656	1205	1781	17093	118
$FWHM$	(0.80)	0.59	0.53	0.58	0.58	0.52	0.52
Si XII v	-64	-84	-54	17	-6	-40	-10
I	2756	1847	839	1378	2818	16748	63
$FWHM$	0.59	0.55	0.50	0.55	0.51	0.50	0.50
Fe XIX v	-141	-140	-56	22	-13	-26	-
I	294	272	694	1271	2721	7544	≤ 0.5
$FWHM$	0.68	0.65	0.56	0.59	0.57	0.55	-

magnetic field (Figure **??**). We mentioned that RHESSI emission was also shifted and confirmed successive reconnections and favouring the fast brightening of the ribbon. The points A and B were reached by CDS at the time of the new bursts of the flare (15:33-15:35 UT) and correspond to an impulsive phase of the flare.

For the analysis of the Hα Dopplershifts we used the observations of VTT/MSDP obtained at 15:30-15:36 UT. We selected areas (Fig. 10) corresponding to the regions observed by SOHO/CDS (see Fig. 11). Regions 6,7,8 in the Hα spectra correspond to region A in the CDS spectra; 4,5 to region B; and 3 to region L1. These regions were not observed at the same time than CDS because of the opposite direction of the scanning of these two instruments. Thus it is not possible to compare directly the velocities.

The profiles in areas 1 and 2 are observed nearly at the onset of the flare. They are very flat or asymmetric and cannot be fitted with satisfactory quality because the profile cover a rather small wavelength range (±0.6Å). Nevertheless, the shape of the profiles is consistent with strong downflows. The other regions 6,7,8 are observed during the gradual phase and exhibit similar shape as the profiles analysed in the previous paper (Berlicki et al. 2005) by using non-LTE radiative transfer codes.

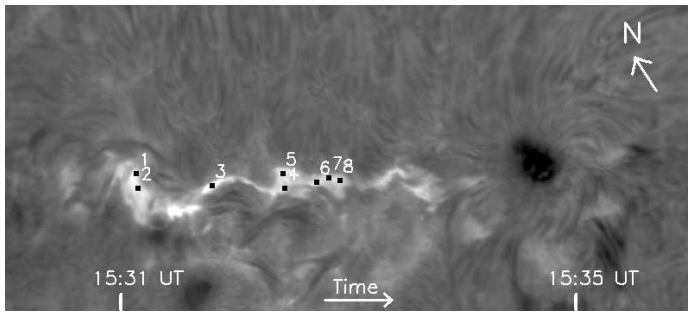

Fig. 10. VTT/MSDP image of AR 0162 taken between 15:30 and 15:36 UT with dots which mark the areas where the Hα line profiles were obtained. The timing and scanning direction are also indicated.

5. Discussion and conclusions

During a coordinated observing campaign, a compact and short-duration M1.0 flare was observed from the ground and in space using spectrographs.

The SOHO/CDS and the VTT/MSDP instruments do allow us to make detailed studies of e.g. the velocities in the ribbons over a wide range of temperatures (10^4 K to $8 \cdot 10^6$ K). However, due to the scanning method of the spec-

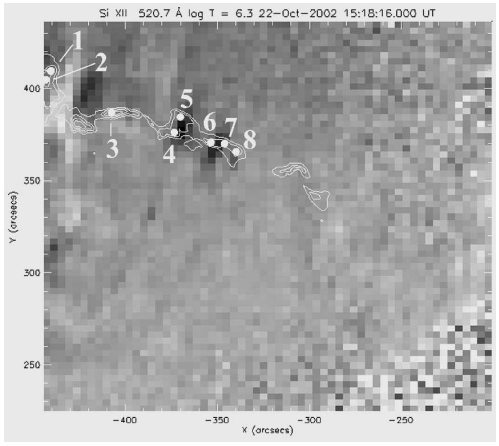

Fig. 11. SOHO/CDS velocity map in the Si XII 520.7 Å line obtained between 15:18 and 15:43 UT. The darker structures represent upflows. The dots (1-8) mark the areas where the Hα line profiles were obtained The contours represent the Hα flare ribbons as observed by VTT during 15:30-15:36 UT.

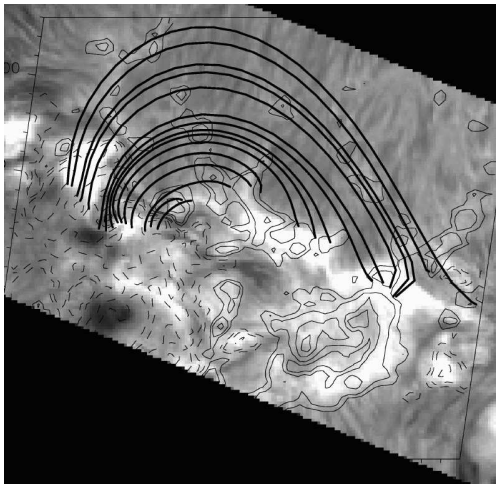

Fig. 12. Extrapolated field lines over the active region explaining the fast propagation of the brightening of the flare ribbon by the rise of the emerging flux, in the plane is represented the photospheric longitudinal magnetic field observed with THEMIS in the Na D1 line

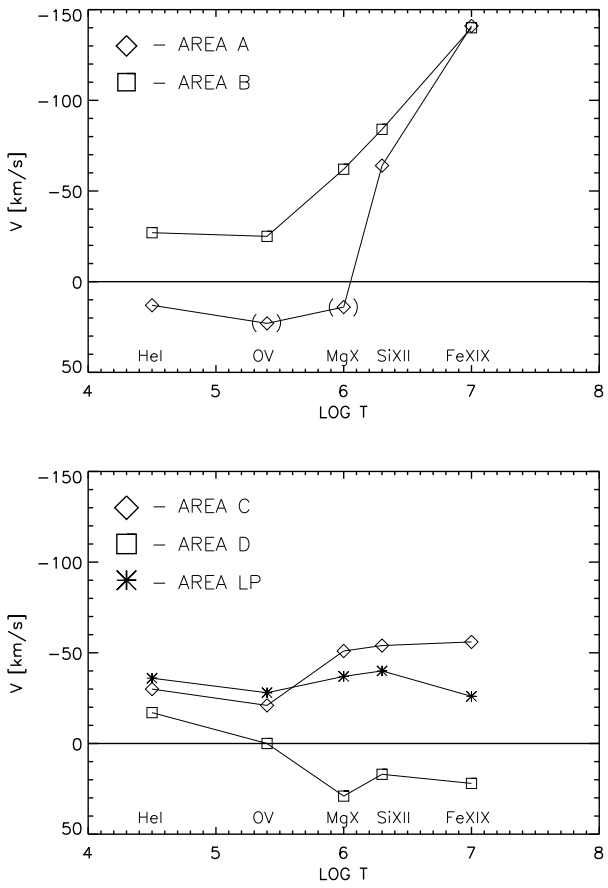

Fig. 13. Flows observed in flare kernels over a large temperature range for different CDS lines: strong blue-shifts in regions A and B for hot lines, weak blueshifts in regions C,and LP, slight redshifts in region D. The error bar is +/- 10 km/s

trographs, we were only not able to obtain spectra from the ribbons during the same phase of the flare. Nontheless we are able to make some accurate measurements of velocities over a range of temperatures, for which we have proposed an explanation. We concentrate this paper mainly on SOHO/CDS flow analysis.

CDS has measured flows in this flare in spectral lines formed over a range of temperatures (log T=5.4-6.9) with an accuracy $\simeq$10 km/s. We find upflows in 'hot' lines that are concentrated in small spatial areas, at the footpoints of coronal/flare loops. Stronger upflows are in the Fe XIX line, indicating that most of the action takes place in the hotter lines.

The large broadenings of the Fe XIX line are in fact indicative of the presence of turbulent motions, in addition to the overall flows. The co-spatiality between the CDS Fe XIX and the TRACE 195 Å emissions suggests that the bulk of the TRACE 195 Å emission at the flare site is due to Fe XXIV.

We selected the areas in CDS which exhibit strong flows. The areas (A,B) that were observed simultaneously by CDS during the peak X-ray emission presented blueshifts. The blueshifts are of the order of 27 km/s in He I, 60 – 88 km/s in Mg X, Si XII, and 140 km/s in Fe XIX in region B. Region A shows slight downflows in the cooler lines.

These regions are relatively far from the flare onset site (location of a small emerging dipole) but they became bright in 2 or 3 minutes after the onset of the flare and this rapid propagation could be explained by a chain of reaction of successive reconnections in the high corona as the emerging flux field lines reconnected with higher and higher preexisting magnetic field.

We suggest that the upflows observed in hot lines in A and B correspond to the so called "explosive evaporation" and the slight downflow observed in cooler lines is due to the overpressure of the chromosphere and even the transition region can be disturbed if that region is thick enough. An important diagnostic tool available with spectroscopic

instruments is the possibility of measuring electron densities over a range of temperatures. We were able to use the CDS O IV diagnostic lines to obtain electron densities of the order of 10^{11} cm^{-3} for the regions A,B. These are somewhat lower that the values of 10^{12} cm^{-3} derived from the Hα data but relatively high compared to the quiet sun electron density (1 or 2 orders more). The exponential increase of the velocity versus the temperature should give constrains to the modelling of the atmosphere above the ribbons.

The eastern parts of the ribbons (areas C, D, LP in the CDS image) are closest to the onset site of the flare but are reached ten minutes later than the onset of the flare. Areas C and and LP exhibited upflows between -30 to -55 km/s according to the temperature of formation of lines with a slight increase versus temperature. Such upflows could correspond to the so called "gentle evaporation" (Fisher et al 1985, Schmieder et al 1987). When the flux associated with non-thermal electrons is low or the non-thermal electrons are not accelerated, then only a weak chromospheric evaporation takes place. Antiochos & Sturrock (1978) suggested that the gentle chromospheric evaporation may occur after the primary energy release when the non-thermal electron flux has stopped. This evaporation could be driven by the large conductive heat flux from a high-temperature flare plasma contained in magnetic tubes above the chromosphere. The small downflows observed in point D are ambiguous and difficult to be explained in this context. Their low values are at the limit of the error bars.

The Hα ribbons are not observed simultaneously with CDS even their observations times are overlapping. The scanning of both instruments were done in opposite directions thus the kernels are not reached at the same time. Therefore it is difficult to have a direct comparison. The asymmetry of Hα line profiles in points 1 and 2 suggests some redshifts of the chromospheric plasma. These profiles were observed at 15:31 UT. This time corresponds to the increase of the GOES soft X-ray flux and this redshift could correspond to the flow that is expected for cool plasma during the impulsive phase. The Hα line profiles in points 5, 6, 7,8 are similar to those analysed by Berlicki et al 2004 during a later phase of this flare. The Dopplershifts derived from the profiles of Hα using a non-LTE radiative transfer code with a flare model correspond to small upflows (2 to 10 km/s) (Berlicki et al. 2005) and could correspond to the "gentle evaporation" observed during the gradual phase of flare in the ribbons.

Other authors (e.g. Brosius & Phillips 2004) have adopted a different observing approach, i.e. to fix the slit position and rely on the imaging instruments to study the morphology of an event. The slit was apparently fortuitously positioned right where the flare took place but they have no indication of the 2D behaviour of the flare.

Our observing campaign and analysis emphasises the importance of combining chromospheric and coronal observations in order to understand the dynamics of a solar flare. It is also essential to use spectroscopic observations to obtain an unambiguous determination of the plasma properties. With this set of observations, we were able to get the exponential variation of the velocity of flaring plasma with temperature during chromospheric evaporation (the "gentle and the explosive" evaporations). The main problem with scanning instruments like VTT/MSDP and CDS is to be in the right place at the right time! Neither the scanning approach or the sit-and-stare approach is entirely satisfactory. We look to future projects, such as SOLAR-B, which will enable us to study active regions and flares in much more detail through all layers of the solar atmosphere.

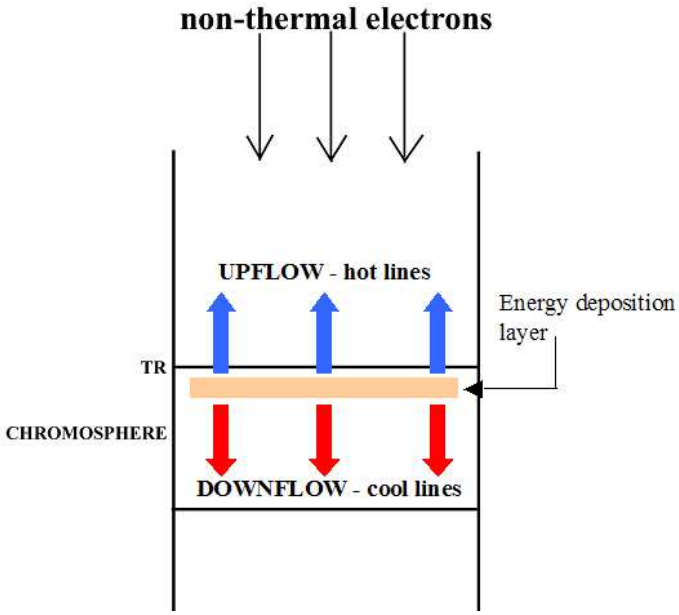

Fig. 14. Sketch of the precipitation of the electrons from the site of reconnection towards the low atmosphere and the expected flows according the temperature of formation of the observed lines.

Acknowledgements. GDZ and HEM acknowledge support from PPARC.

This research was partially supported by the European Commission through the RTN programme ESMN (European Solar Magnetism Network, contract HPRN-CT-2002-00313). AB and BS are members of ESMN. SOHO is a project of international collaboration between ESA and NASA. These observations were performed during a MEDOC campaign (JOP 157). The magnetic field extrapolations were obtained from the code FROMAGE (FRench Online MAGnetic Extrapolations) We acknowledge the use of the SURF, TRACE, SOHO on-line databases.

References

Antiochos, S. K. & Sturrock, P. A. 1978, ApJ, 220, 1137

Antonucci, E., Gabriel, A. H., Acton, L. W., et al. 1982, Sol. Phys., 78, 107

Antonucci, E., Gabriel, A. H., & Dennis, B. R. 1984, ApJ, 287, 917

Bentley, R. D., Doschek, G. A., Simnett, G. M., et al. 1994, ApJ, 421, L55

Berlicki, A. & Heinzel, P. 2004, A&A, 420, 319
Berlicki, A., Heinzel, P., Schmieder, B., Mein, P., & Mein, N. 2005, A&A, 430, 679
Berlicki, A., Schmieder, B., Vilmer, N., Aulanier, G., & Del Zanna, G. 2004, A&A, 423, 1119
Bradshaw, S. J., Del Zanna, G., & Mason, H. E. 2004, A&A, 425, 287
Brosius, J. W. & Phillips, K. J. H. 2004, ApJ, 613, 580
Czaykowska, A., de Pontieu, B., Alexander, D., & Rank, G. 1999, ApJ, 521, L75
Del Zanna, G., Berrington, K. A., & Mason, H. E. 2004, A&A, 422, 731
Del Zanna, G. & Bromage, B. J. I. 1999, J. Geophys. Res., 104, 9753
Del Zanna, G., Bromage, B. J. I., Landi, E., & Landini, M. 2001, A&A, 379, 708
Del Zanna, G., Gibson, S. E., Mason, H. E., Pike, C. D., & Mandrini, C. H. 2002a, Advances in Space Research, 30, 551
Del Zanna, G. & Mason, H. E. 2004, A&A, in press
Del Zanna, G., Mason, H. E., & Foley, C. 2002b, in ESA SP-506: Solar Variability: From Core to Outer Frontiers, 585–588
Ding, M. D., Qiu, J., & Wang, H. 2002, ApJ, 576, L83
Doschek, G. A., Kreplin, R. W., & Feldman, U. 1979, ApJ, 233, L157
Fisher, G. H. 1987, ApJ, 317, 502
Fisher, G. H., Canfield, R. C., & McClymont, A. N. 1985a, ApJ, 289, 434
Fisher, G. H., Canfield, R. C., & McClymont, A. N. 1985b, ApJ, 289, 425
Fisher, G. H., Canfield, R. C., & McClymont, A. N. 1985c, ApJ, 289, 414
Forbes, T. G., Malherbe, J. M., & Priest, E. R. 1989, Sol. Phys., 120, 285
Gibson, S. E., Fletcher, L., Del Zanna, G., et al. 2002, ApJ, 574, 1021
Heinzel, P. 1995, A&A, 299, 563
Heinzel, P., Karlicky, M., Kotrc, P., & Svestka, Z. 1994, Sol. Phys., 152, 393
Ichimoto, K. & Kurokawa, H. 1984, Sol. Phys., 93, 105
Kosovichev, A. G. & Zharkova, V. V. 2001, ApJ, 550, L105
Lawson, K. D. & Peacock, N. J. 1980, Journal of Physics B Atomic Molecular Physics, 13, 3313
Mason, H. E., Shine, R. A., Gurman, J. B., & Harrison, R. A. 1986, ApJ, 309, 435
Mihalas, D. 1978, Stellar atmospheres /2nd edition/ (San Francisco, W. H. Freeman and Co., 1978. 650 p.)
Nejezchleba, T. 1998, A&AS, 127, 607
Sandlin, G. D., Brueckner, G. E., Scherrer, V. E., & Tousey, R. 1976, ApJ, 205, L47
Schmieder, B., Forbes, T. G., Malherbe, J. M., & Machado, M. E. 1987, ApJ, 317, 956
Schmieder, B., Malherbe, J. M., Simnett, G. M., Forbes, T. G., & Tandberg-Hanssen, E. 1990, ApJ, 356, 720
Svestka, Z. 1976, Geophysics and Astrophysics Monographs, 8
Teriaca, L., Falchi, A., Cauzzi, G., et al. 2003, ApJ, 588, 596
Warren, H. P. & Doschek, G. A. 2005, ApJ, 618, L157
Widing, K. G. 1978, ApJ, 222, 735
Zarro, D. M., Slater, G. L., & Freeland, S. L. 1988, ApJ, 333, L99